Acta Crystallographica Section A
Foundations of Crystallography
ISSN 0108-7673

Received 22 August 2008
Accepted 24 September 2009

X-ray constrained unrestricted Hartree–Fock and Douglas–Kroll–Hess wavefunctions

Martin Hudák,[a] Dylan Jayatilaka,[b] Lucia Perašínová,[a] Stanislav Biskupič,[a] Jozef Kožíšek[a] and Lukáš Bučinský[a]*

[a]Slovak University of Technology, Department of Physical Chemistry, SK-81237 Bratislava, Slovakia, and [b]The University of Western Australia, School of Biomedical, Biomolecular and Chemical Sciences, WA 6009, Australia. Correspondence e-mail: lukas.bucinsky@stuba.sk

The extension of the X-ray constrained (XC) wavefunction approach to open-shell systems using the unrestricted Hartree–Fock formalism is reported. The XC method is also extended to include relativistic effects using the scalar second-order Douglas–Kroll–Hess approach. The relativistic effects on the charge and spin density on two model compounds containing the copper and iron atom are reported. The size of the relativistic effects is investigated in real and reciprocal space; in addition, picture-change effects are investigated and discussed for the isolated Cu atom. It is found that the relativistic terms lead to changes in the densities that are much smaller than those from the X-ray constraint. Nevertheless, the use of the relativistic corrections in the *ab initio* model always leads to an improvement in the agreement statistics. An interesting result of the unrestricted XC technique is the possibility of obtaining experimentally derived spin densities from X-ray data.

1. Introduction

It is interesting to study transition metal complexes using X-ray charge density methods because they promise the possibility of rationalizing novel modes of bonding and catalysis, often involving unpaired electrons in *d* shells. However, transition metals are not fully suitable for charge density analysis because most of the X-ray scattering comes from the core electrons (Stevens & Coppens, 1976). Traditionally these core electrons are not interesting from a chemical bonding point of view. Nevertheless, the importance of core electrons for charge density measurements demands that they be treated properly. With growing atomic weight, relativistic effects start to become significant, and these effects contribute to the distribution of charge density. Unfortunately the dominance of the core electrons for the X-ray scattering and the complexity of bonding in transition metal complexes makes it difficult to model the valence electron density by traditional multipole models. Flexible radial functions are necessary (Figgis *et al.*, 1993) and the additional flexibility requires a data quality that may not always be available.

The X-ray constrained (XC) wavefunction approach offers a solution to the difficulties of modelling transition metal complexes. The idea of the approach is to constrain an *ab initio* isolated molecule wavefunction to reproduce the structure factors from the experiment (Jayatilaka, 1998; Jayatilaka & Grimwood, 2001; Grimwood & Jayatilaka, 2001; Grimwood *et al.*, 2003). In this way for transition metal systems the core electrons can be modelled properly (with the appropriate choice of Hamiltonian), thus allowing the maximum amount of information on the valence charge density to be extracted from the X-ray data.

This paper describes the extension of the XC wavefunction approach to open-shell systems at the unrestricted level (Whitton, 2004). Importantly, this extension allows the spin density to be derived (according to the usual rules of quantum mechanics) from the XC wavefunction. In other words, the spin density is derived indirectly from the charge density measurements and the XC wavefunction model. In addition, the XC method is extended to include relativistic effects which are important to core electrons of heavy-atom systems. Apart from an improvement of the model for the core electrons, another reason for introducing relativistic effects is the motivation to quantify the extent of relativity recovered by the X-ray constraint. From the several quasi-relativistic Hamiltonians (van Lenthe *et al.*, 1993, 1994; Barysz & Sadlej, 2001; Dyall & van Lenthe, 1999; Ilias & Saue, 2006) the scalar second-order Douglas–Kroll–Hess (DKH2) Hamiltonian (Hess, 1985; Wolf *et al.*, 2002*a*,*b*, 2004) has been adopted. The general advantage of the scalar DKH2 Hamiltonian is that it can be easily implemented in the non-relativistic quantum chemistry codes. Moreover, systematic improvement beyond the second order is possible (Nakajima & Hirao, 2000; Reiher & Wolf, 2004*a*,*b*).

The disadvantage of the DKH approach is that there is a picture change present in the wavefunction. It must be taken into account when molecular properties, electron densities and structure factors are calculated. The so-called picture-change effect (PCE) in electron densities has been addressed by

several authors (Eickerling *et al.*, 2007; Reiher, 2007; van Wüllen & Michauk, 2005; Mastarlez *et al.*, 2008), but to our knowledge not in terms of the structure factors which are important for the XC method. Therefore in this paper we also examine the PCE in the atomic scattering factor.

The arrangement of this paper is as follows. First we provide the theoretical background for the XC unrestricted Hartree–Fock (UHF) method, XC–UHF spin densities, the DKH method and the PCE. After some computational details the PCE is investigated in detail for the copper atom, followed by an investigation of relativistic effects in compounds containing 3*d* elements (iron and copper). The first compound under study is [Fe(salpet)Cl] (Šalitroš *et al.*, 2009), shown in Fig. 1(*a*), where salpet is the abbreviation for the $OC_6H_4CHN(R_1)NH(R_2)NCHC_6H_4O$ ligand, with R_1 = $CH_2CH_2CH_2$ and R_2 = CH_2CH_2. The second model compound, [CuL_2] (Boča *et al.*, 1996), shown in Fig. 1(*b*), contains the chelate ligand L = $N[C(NH)–OCH_3]_2$. Both compounds are studied with and without the X-ray constraint. Agreement statistics, the relativistic and XC effects to the total energy of the compounds, and plots of electron and spin density are displayed. Conclusions and an outlook are given in the final section.

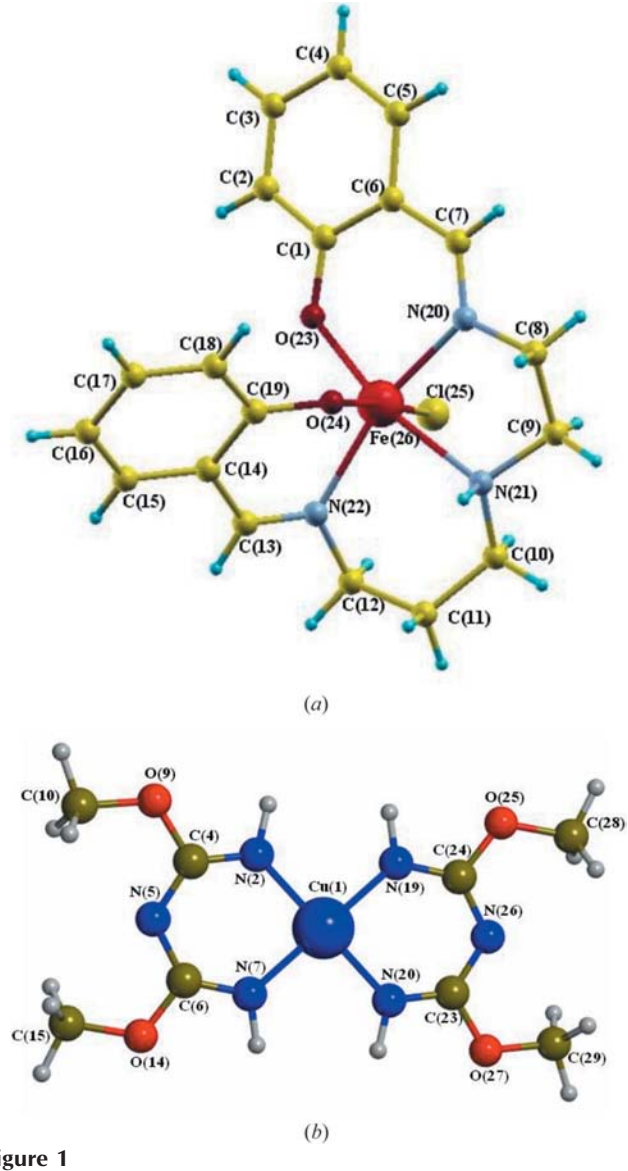

Figure 1
Structures of the studied compounds [Fe(salpet)Cl] (*a*) and [CuL_2] (*b*).

2. Theoretical background

2.1. XC-UHF approach

The XC wavefunction is a compromise between the wavefunction with lowest energy E and the wavefunction with best agreement χ^2 between the experimental and calculated structure factors. For the case of a UHF wavefunction we extended the usual restricted approach by minimizing the Lagrange functional

$$L(\mathbf{c}^\alpha, \mathbf{c}^\beta, \boldsymbol{\varepsilon}^\alpha, \boldsymbol{\varepsilon}^\beta, \lambda) = \underbrace{E(\mathbf{c}^\alpha, \mathbf{c}^\beta) - \mathrm{Tr}\left[(\mathbf{c}^\alpha)^+ S\,\mathbf{c}^\alpha - 1\right]\boldsymbol{\varepsilon}^\alpha - \mathrm{Tr}\left[\left(\mathbf{c}^\beta\right)^+ S\,\mathbf{c}^\beta - 1\right]\boldsymbol{\varepsilon}^\beta}_{\text{UHF}} + \underbrace{\lambda\left[\chi^2(\mathbf{c}^\alpha, \mathbf{c}^\beta) - \Delta\right]}_{\text{X-ray constraint}} \quad (1)$$

with respect to the α and β molecular orbital coefficients $\mathbf{c}^\alpha$ and $\mathbf{c}^\beta$, respectively. Here E is the UHF energy, S is the overlap matrix in the chosen basis set and $\boldsymbol{\varepsilon}^\alpha$ and $\boldsymbol{\varepsilon}^\beta$ are the usual Lagrange multipliers, which introduce the molecular orbital (MO) orthonormality condition into the UHF equations. Δ is the desired error of the χ^2 value; χ^2 is the agreement statistic through which the experimental X-ray data are introduced,

$$\chi^2 = \frac{1}{N_\mathrm{r} - N_\mathrm{p}} \sum_j^{N_\mathrm{r}} \frac{\left(F_j - F_j^X\right)^2}{\sigma_j^2}. \quad (2)$$

Here N_r is the number of measured reflections and N_p is the number of adjustable fitting parameters (normally equal to 1 for parameter λ), and σ_j is the experimental error associated with the measured structure factor F_j. F_j^X is the predicted structure-factor magnitude from the model wavefunction,

$$F_j^X = \xi F_j^\mathrm{C}, \quad (3)$$

where ξ is an overall scale factor which adjusts the calculated structure-factor magnitude F_j^C to the scale used in the experiment. It may also include an angle-dependent extinction correction (not used in this paper).

The derivatives of the Lagrange functional (1) with respect to $\mathbf{c}^\alpha$ and $\mathbf{c}^\beta$ lead to the XC-UHF equations,

$$\begin{aligned} \tilde{\mathbf{F}}^\alpha \mathbf{c}^\alpha &= S\,\mathbf{c}^\alpha \boldsymbol{\varepsilon}^\alpha, \\ \tilde{\mathbf{F}}^\beta \mathbf{c}^\beta &= S\,\mathbf{c}^\beta \boldsymbol{\varepsilon}^\beta, \end{aligned} \quad (4)$$

where $\tilde{\mathbf{F}}^\alpha$ and $\tilde{\mathbf{F}}^\beta$ are the modified UHF matrices given by

$$\begin{aligned} \tilde{\mathbf{F}}^\alpha &= \mathbf{F}^\alpha - \lambda \mathbf{C}, \\ \tilde{\mathbf{F}}^\beta &= \mathbf{F}^\beta - \lambda \mathbf{C}, \end{aligned} \quad (5)$$

and where $\mathbf{F}^\alpha$ and $\mathbf{F}^\beta$ are the usual UHF matrices (Szabo & Ostlund, 1989). The constraint matrix $\mathbf{C}$ is given by

$$\mathbf{C} = \frac{2}{N_\mathrm{r} - N_\mathrm{p}} \sum_j^{N_\mathrm{r}} \left(\frac{F_j - F_j^X}{\sigma_j} \right) \left[\frac{\left(F_j^X\right)^* \mathbf{I}_j - F_j^X \mathbf{I}_j^\dagger}{2\left|F_j^X\right|} \right]. \quad (6)$$

The $\mathbf{I}_j$ matrix contains the Fourier-transformed basis function pairs $g_\mu(\mathbf{r})g_\nu(\mathbf{r})$ which have been summed over all symmetry-related molecules centred at positions $\mathbf{r}_m$ in the unit cell, and being thermally averaged by multiplication with an appropriate Debye–Waller factor,

$$I_{\mu\nu,j} = \sum_{m=1}^{N_m} \exp\left(2\pi i \mathbf{q}_j \cdot \mathbf{r}_m\right) T_{\mu\nu} \int g_\nu^*(\mathbf{r}) g_\mu(\mathbf{r}) \exp\left(i \mathbf{R}_m^T \mathbf{q}_j \cdot \mathbf{r}\right) \mathrm{d}\mathbf{r}. \quad (7)$$

The $\mathbf{I}_j$ matrix is independent of molecular coefficients. $\mathbf{R}_m^T$ is a rotation matrix generating the mth symmetry-equivalent molecule from the first one; $\mathbf{r}_m$ is the position of the origin of the mth symmetry-equivalent molecule in the unit cell, $T_{\mu\nu}$ is the Debye–Waller factor assigned to the basis function pair $(\mu\nu)$ and $\mathbf{q}_j$ is the scattering vector for the jth reflection (Jayatilaka, 1998; Jayatilaka & Grimwood, 2001; Grimwood *et al.*, 2003). A Cartesian axis system has been used. The XC-UHF equations (4) are solved in the usual self-consistent way.

2.2. XC-UHF spin density

One of the advantages of the XC wavefunction approach is that, once the XC wavefunction has been obtained, derived properties can easily be obtained from it according to the standard rules of quantum mechanics (normally these properties will be obtained as expectation values of the wavefunction). For example, familiar properties directly related to the electron density, such as atomic charges and electrostatic potentials, can be obtained (Grimwood & Jayatilaka, 2001). Even more unusual properties such as the Fermi hole mobility function, kinetic energy densities, electron localization functions (Jayatilaka & Grimwood, 2004), refractive indices or NLO response properties (Whitten *et al.*, 2006; Jayatilaka *et al.*, 2009) can be derived from the XC wavefunction as well. It is not possible to obtain these more unusual properties from a multipole model of the electron density: some kind of quantum mechanical or wavefunction-based model is needed. (It is worth pointing out that regions of negative electron density cannot occur in the XC approach, whereas such regions are not unusual in a standard multipole approach.)

It is important to realize that the more unusual derived properties by the XC approach are not measured directly in the X-ray experiment; experiment only yields structure-factor magnitudes for the thermally smeared electron density. Rather, these properties are obtained from the model wavefunction and/or electron density fitted to these experimentally determined structure-factor magnitudes. The possibility of deriving any of these properties from the X-ray data ultimately rests with the fact that the electron density contains enough information within itself to provide this information (Hohenberg & Kohn, 1964; Jayatilaka & Grimwood, 2001). The reliability of any XC-derived property must be tested on a case-by-case basis, as must the effect of the X-ray data on that property.

In the present case, for open-shell systems, it is straightforward to obtain an experimentally derived unpaired electron density (spin density) from the XC wavefunction. The unpaired electron density is defined as

$$\rho_s = \rho_\alpha - \rho_\beta. \quad (8)$$

The alpha (ρ_α) and beta (ρ_β) densities are obtained from

$$\rho_\alpha = \sum_{\mu,\nu} D_{\mu\nu}^\alpha g_\mu(r) g_\nu(r), \quad (9)$$

$$\rho_\beta = \sum_{\mu,\nu} D_{\mu\nu}^\beta g_\mu(r) g_\nu(r), \quad (10)$$

where $g_\mu(r)$ and $g_\nu(r)$ are the atomic orbital basis functions and D^α and D^β are the alpha and beta density matrices, respectively, given by

$$D_{\mu\nu}^\alpha = \sum_i^{n_\alpha} c_{i\mu}^{\alpha *} c_{i\nu}^\alpha, \quad (11)$$

$$D_{\mu\nu}^\beta = \sum_i^{n_\beta} c_{i\mu}^{\beta *} c_{i\nu}^\beta, \quad (12)$$

with $c_{i\mu}^\alpha$, $c_{i\nu}^\alpha$, $c_{i\mu}^\beta$ and $c_{i\nu}^\beta$ being the MO coefficients. The integral of the spin density gives the number of unpaired electrons,

$$n_\alpha - n_\beta = \int \rho_s(\mathbf{r}) \, \mathrm{d}\mathbf{r}. \quad (13)$$

It is our goal to present UHF spin densities defined by (8) and to test the effect of the X-ray constraint on them. We do not intend in this paper to validate the results with independent measurements; that will be for future work.

The UHF wavefunctions used in this paper may not be ideal for the production of spin densities. One reason often cited is that single-determinant UHF wavefunctions are not eigenfunctions of the total spin operator $\hat{S}^2$ (Szabo & Ostlund, 1989); this is because the wavefunction of a given multiplicity gains contributions from states of higher multiplicity (Szabo & Ostlund, 1989). The exact wavefunction is known to be an eigenfunction of $\hat{S}^2$ when effects of spin–orbit coupling are ignored. Because of this, so-called spin contamination may be the result. The spin contamination can be removed by using a restricted open-shell approach, *i.e.* by using the same molecular orbitals for alpha and beta spin (Cassam-Chenaï & Chandler, 1993), or else it can be removed by applying a constraint to remove the spin contamination (Andrews *et al.*, 1991). Another feature of the UHF method is the presence of regions of negative spin density; these do not occur in single-determinant wavefunctions which are eigenfunctions of $\hat{S}^2$. Although use of different spatial orbitals for the alpha and beta molecular orbitals on the one hand introduces regions of negative spin density and spin contamination, on the other the UHF approach leads to a lower-energy wavefunction, *i.e.* leads to a wavefunction with better overlap with the exact wavefunction.

If further the UHF theory is regarded as a branch of the density functional theory (Parr & Yang, 1989), then it appears theoretically more acceptable to use an unrestricted approach than a restricted one (Pople *et al.*, 1995). For example, it has already been shown that, at the level of the unrestricted

density functional theory (UDFT), quite reasonable spin densities are obtained (Aebersold *et al.*, 1998; Aronica *et al.*, 2007) although the UDFT method appears less sensitive to spin contamination. Because of the uncertainty surrounding the role of spin contamination, and the relative simplicity of the UHF approach, we have pursued it here in this paper, but its limitations must be kept in mind.

2.3. The DKH Hamiltonian

The scalar DKH2 (Hess, 1985; Wolf *et al.*, 2002*a*,*b*, 2004; Reiher & Wolf, 2004*a*,*b*) is nowadays a widely used approximation to the Dirac–Coulomb Hamiltonian (DCH) (Schwerdtfeger, 2002; Dyall & Faegri, 2007). Therefore to understand the DKH approach we start with the DCH. The one-electron DCH is given by

$$\hat{h}_{\rm DCH} = \begin{pmatrix} V & c\boldsymbol{\sigma}\cdot\hat{\mathbf{p}} \\ c\boldsymbol{\sigma}\cdot\hat{\mathbf{p}} & V - 2mc^2 \end{pmatrix}, \tag{14}$$

where c is the speed of light, $\hat{\mathbf{p}}$ is the momentum operator, m is the electron rest mass and V is the potential energy of the electron–nucleus Coulomb interaction. The term mc^2 has been subtracted from the DCH within (14) to align it with the non-relativistic energy scale. $\boldsymbol{\sigma}$ is the vector of Pauli's spin matrices,

$$\boldsymbol{\sigma}_x = \begin{pmatrix} 0 & 1 \\ 1 & 0 \end{pmatrix}, \quad \boldsymbol{\sigma}_y = \begin{pmatrix} 0 & -i \\ i & 0 \end{pmatrix}, \quad \boldsymbol{\sigma}_z = \begin{pmatrix} 1 & 0 \\ 0 & -1 \end{pmatrix}. \tag{15}$$

Unlike the non-relativistic (NR) Hamiltonian, the DCH is a four by four matrix which explicitly treats spin, but unfortunately introduces besides the positive energy also the troublesome negative energy states. One of the major computational demands of the calculations at the DCH level is due to the presence of the additional degree of freedom of negative energy states.

The essential idea behind the DKH Hamiltonian is the block diagonalization of the DCH using a unitary transformation U to decouple the positive and negative energy states,

$$\hat{H}_{\rm decoupled} = U\hat{h}_D U^{+} = \begin{pmatrix} h_{+} & 0 \\ 0 & h_{-} \end{pmatrix}, \tag{16}$$

where the h_{+} block corresponds to a two-component Hamiltonian having only positive energy eigenstates and is of primary interest for chemistry. It is used in place of the usual one-electron NR Hamiltonian. The h_{-} block of the negative branch of energy spectra in the decoupled Hamiltonian in (16) is simply ignored (Reiher, 2006). The two-component Hamiltonian h_{+} can be split into spin-free and spin-dependent terms (Hess, 1985; Wolf *et al.*, 2002*a*,*b*, 2004). Retaining only the spin-free terms of h_{+} leads to the one-component or scalar or spin-free DKH Hamiltonian.

The unitary matrix U has no closed formulation in the case of the DKH approach and is formed as a product of a series of unitary matrices U_i,

$$U = \ldots U_2 U_1 U_0. \tag{17}$$

The zero-order transformation U_0 in (17) is the free particle Foldy Wouthuysen (fpFW) transformation (Foldy & Wouthuysen, 1950). This is followed by the Douglas–Kroll (DK) transformations U_i (i = 1, 2, ...) (Douglas & Kroll, 1974). In the case of the DKH2 Hamiltonian only the fpFW U_0 and DK first-order U_1 transformations are retained.

The fpFW transformation U_0 actually introduces operators which are non-local in coordinate space but which are easily evaluated in the momentum space representation (Hess, 1985). The basic idea of how to implement the DK Hamiltonian into existing quantum chemistry codes, using the ordinary Gaussian basis sets in Cartesian coordinate space, has come from Hess and co-workers (Buenker *et al.*, 1984; Hess, 1985), and we refer the reader to the literature for further details on the implementation (Wolf *et al.*, 2002*a*,*b*, 2004; Reiher, 2006). One minor but crucial detail needs to be highlighted, namely that the primitive uncontracted Gaussian basis is used to represent the momentum eigenfunctions in the expansion of the resolution of the identity; for example, equation (A6) in Wolf *et al.* (2002*b*), which is used repeatedly in the DKH method.

2.4. Picture-change effect

The transition from the DCH to the decoupled DKH Hamiltonian is associated with a change in the wavefunction of the systems (Wolf & Reiher, 2006*a*,*b*),

$$\begin{aligned} \left\langle \Psi \middle| \hat{h}_D | \Psi \right\rangle &= \left\langle \Psi \middle| U^{+} U \hat{h}_D U^{+} U | \Psi \right\rangle \\ &= \left\langle U\Psi \middle| U \hat{h}_D U^{+} | U\Psi \right\rangle \\ &= \left\langle \tilde{\Psi} \middle| \hat{H}_{\rm decoupled} \middle| \tilde{\Psi} \right\rangle, \end{aligned} \tag{18}$$

where

$$\tilde{\Psi} = U\Psi. \tag{19}$$

This change of wavefunction is known as the picture change. It should be noted that the wavefunction Ψ is associated with $\hat{h}_D$ while $\tilde{\Psi}$ is associated with the modified operator $\hat{H}_{\rm decoupled} = U\hat{h}_D U^{+}$. Likewise, if an operator $\hat{X}$ is used with Ψ then a modified operator $U\hat{X}U^{+}$ should be used with $\tilde{\Psi}$. Unfortunately, it is often the case that $\tilde{\Psi}$ is used with the unmodified operator $\hat{X}$, which leads to an error in the expectation value of operator $\hat{X}$, denoted as the picture-change effect (PCE). The PCE in the expectation value of operator $\hat{X}$ (Wolf & Reiher, 2006*a*,*b*; Barysz & Sadlej, 2001) can be given as the difference

$$\mathrm{PCE}(X) = \left\langle \tilde{\Psi} \middle| U\hat{X}U^{+} \middle| \tilde{\Psi} \right\rangle - \left\langle \tilde{\Psi} \middle| \hat{X} \middle| \tilde{\Psi} \right\rangle. \tag{20}$$

The PCE is significant for properties related to the electrons localized in the nuclear region (*i.e.* electron density), which is the high energetic part in the atoms (Mastarlez *et al.*, 2008). Properties like electric field gradient tensors (Barone *et al.*, 2008) or hyperfine coupling (Malkin *et al.*, 2002, 2004) have to be PCE corrected. On the other hand, the electrons in the valence region, *i.e.* electron density (Eickerling *et al.*, 2007; Reiher, 2007; van Wüllen & Michauk, 2005; Mastarlez *et al.*, 2008), and properties which presumably depend on the valence region electrons (bonding electron density) seem to be much less effected by the PCE. The calculations of dipole

moments and polarizabilities (Kellö & Sadlej, 1990, 1995*a*,*b*; Kellö *et al.*, 1996; Norman *et al.*, 2002) have not proved to be significantly influenced by the PCE.

3. Computational details

Here we present details on the relativistic and non-relativistic calculations of the studied compounds [Fe(salpet)Cl] and [CuL_2] and the isolated copper atom ([Ar]$3d^{10}4s^1$); the compounds are shown in Figs. 1(*a*) and 1(*b*). The first octahedral complex denoted [Fe(salpet)Cl] (Šalitroš *et al.*, 2009) contains the Fe(III) atom surrounded by a pentadentate ligand salpet and Cl atom. The whole molecule [Fe(salpet)Cl] comprises the asymmetric unit of the crystal, where salpet is the abbreviation for the $OC_6H_4CHN(R_1)NH(R_2)NCHC_6H_4O$ ligand with $R_1 = CH_2CH_2CH_2$ and $R_2 = CH_2CH_2$. The second model compound under study was the bis[bis(methoxycarbimido)aminato]copper(II) complex (Boča *et al.*, 1996), abbreviated as [CuL_2] with the chelate ligand $L = N[C(NH)OCH_3]_2$. The asymmetric unit is comprised of one of the chelate ligands L and the copper atom. The whole molecule [CuL_2] is produced from the asymmetric unit by an inversion symmetry operation. The labelling of the atoms in Fig. 1 is used within the coming sections. The visualization plane of the two-dimensional densities is defined in the case of [CuL_2] by the copper and N(2), N(7) nitrogen atoms, and in the case of the [Fe(salpet)Cl] compound by the plane defined by the Fe, O(23) and N(20) atoms.

3.1. X-ray data

Details on the X-ray data of the studied compounds are collected in Table 1. The *SHELX97* package (Sheldrick, 2008) was used to perform the refinements of the studied systems. The R factor and the weighted R factor in Table 1 were obtained from the *SHELX97* program (Sheldrick, 2008). Anisotropic atom displacement parameters (ADPs) were used for all non-hydrogen elements. The experimental data were not corrected for secondary extinction. The experimental error σ_j which is present within the χ^2 value in equation (2) is obtained at the experimental data reduction step. The background intensity (signal/noise) is taken into account in σ_j; the main contribution is obtained by calculating the deviation of redundant measurements of a given reflection from their mean value.

3.2. Spin states of the compounds

The central iron(III) in this compound has two possible spin states (multiplicities), namely a low (doublet) and a high (sextet) spin state. An experimental study of Mössbauer spectra (Šalitroš *et al.*, 2009) has shown that the high spin state is the appropriate state in the case of this compound. A UHF/6-31G* calculation unambiguously yielded the lower energy for the high spin state by 104 mhartree (2.84 eV; 245 kJ mol^{-1}) compared with the doublet. The spin state of copper(II) in [CuL_2] is a doublet.

Table 1
Details of the studied compounds [Fe(salpet)Cl] and [CuL_2] obtained from the X-ray experiment and the refinement process.

	[Fe(salpet)Cl]	[CuL_2]
Composition	$C_{19}H_{21}N_3O_3FeCl$	$C_8H_{16}CuN_6O_4$
Formula weight	414.687	323.90
Crystal system	Monoclinic	Monoclinic
Space group	$P2_1/c$	$P2_1/n$
Cell parameters		
a (Å)	11.048 (9)	9.8826 (6)
b (Å)	12.020 (1)	5.7121 (3)
c (Å)	14.263 (1)	11.4037 (8)
β (°)	108.34 (7)	98.893 (5)
V (Å^3)	1797.8	636.00 (7)
Z	4	2
Density, D_c (g cm^{-3})	1.532	1.653
Absorption coefficient (mm^{-1})	1.006	0.784
$F(000)$	860	334
$\sin\theta_{max}/\lambda$ (Å^{-1})	0.6383	1.0901
Refinement method	Full-matrix least-squares on F^2	–
Final R indices, R_1	0.0474	0.0229
wR_2	0.1142	0.0576
Number of reflections	39625	38326

3.3. Basis sets

In the case of the [Fe(salpet)Cl] compound the cc-pVTZ basis set (Balabanov & Peterson, 2005, 2006) was used for the Fe atom at the NR level. At the unrestricted DKH2 (UDKH2) level the DK recontracted cc-pVTZ-DK basis set (Balabanov & Peterson, 2005, 2006) was employed. The cc-pVDZ basis set was used for the lighter elements Cl, O, N, C at the NR level (Dunning, 1989; Woon & Dunning, 1993). At the UDKH2 level the recontracted cc-pVDZ-DK (Peterson *et al.*, 2007) basis set was used. The H atoms were treated in the 6-31G basis set (Hehre *et al.*, 1972) at both the NR and UDKH2 level.

In the case of the [CuL_2] compound the cc-pVDZ basis set (Balabanov & Peterson, 2005, 2006) was used for the Cu atom at the NR level. At the UDKH2 level the cc-pVDZ-DK (Balabanov & Peterson, 2005, 2006) basis set was used. The 6-31G* and 6-31G basis sets (Hehre *et al.*, 1972) were chosen for the remaining atoms (C, N, O and H) of the [CuL_2] complex.

The calculations of the free Cu atom were performed using an uncontracted (primitive) cc-pVDZ basis set (Balabanov & Peterson, 2005, 2006) enlarged by two s and one p high-exponent Gaussians using an even-tempered series.

3.4. XC calculations

The X-ray constrained relativistic (XC-UDKH2) and X-ray constrained non-relativistic (XC-UHF) calculations were performed with successively larger values of λ, by 0.05, for both compounds. The initial guess for the molecular orbital at $\lambda = 0.00$ was taken from the promolecule Fock matrix. λ(max) for [Fe(salpet)Cl] was 0.6; for [CuL_2] it was 0.4. λ(max) was chosen so that the change in the weighted R factor was less than 0.04% for both compounds. In the coming sections any results denoted as XC mean a λ(max) XC calculation. The structure factors used in the XC-UDKH2 calculations were

calculated in the usual way and have not been corrected for the PCE; instead consideration of the PCE in the angular dependence of atomic scattering factors of the Cu atom is presented in §4.1. The ADPs were taken from the multipole refinement of the experimental data. The entire data set was used in the XC-UHF method. Weak negative intensity reflections $F_j < 0$ have been set to zero $F_j = 0.0$ and the sigma value was adjusted appropriately, *i.e.* $\sigma_j \rightarrow \sigma_j + |F_j|$. Corrections for secondary extinction were not applied.

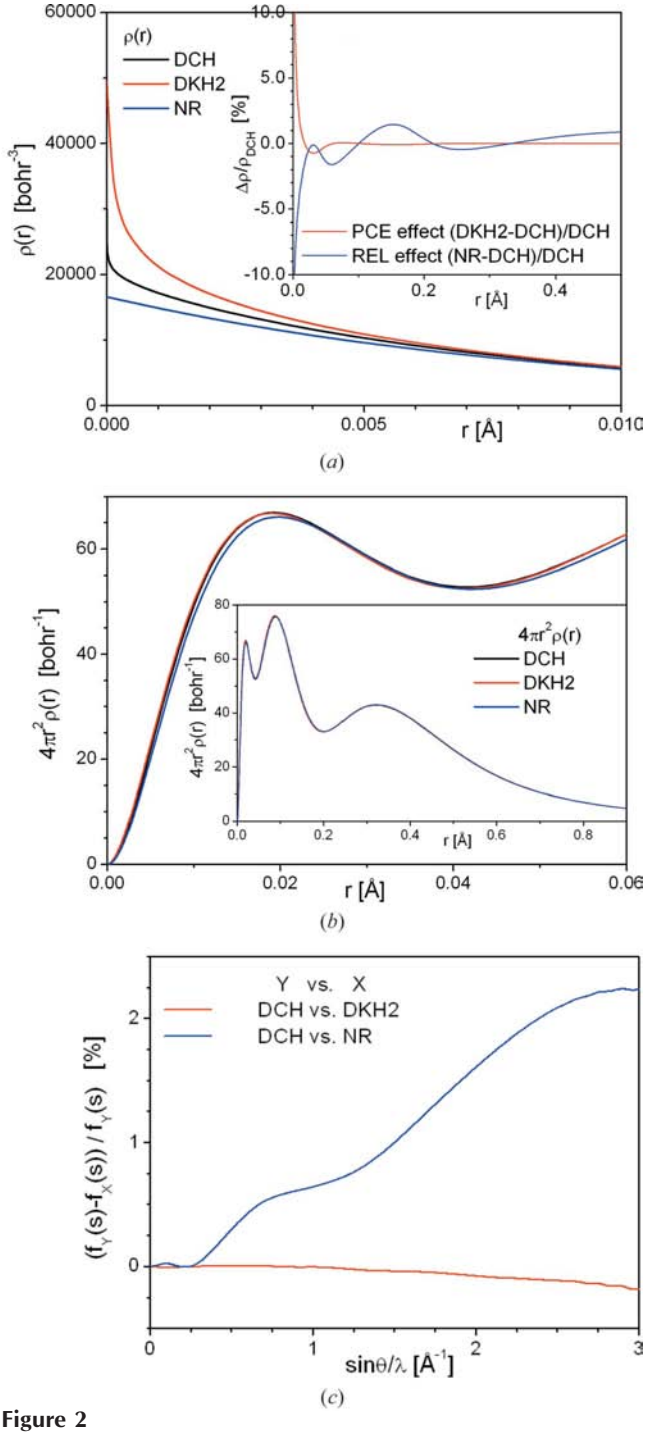

Figure 2
(*a*) Radial distribution of the Cu atom electron density $\rho(r)$ at the DCH, DKH2 and NR level of theory. The inset shows the percentage change in the electron density. (*b*) Integral electron density distribution of the function $4\pi r^2\rho(r)$ of the Cu atom, in the range 0.0 to 0.06 Å. The inset shows the range 0.0 to 0.9 Å. (*c*) Scattering-angle dependence of the relative significance of the PCE and relativistic effects in the atomic scattering factor of the Cu atom comparing the DCH atomic scattering factors.

3.5. Software

The calculations were performed using a modified version of *TONTO* (Jayatilaka & Grimwood, 2000). The new software is available under a free software licence from http://sourceforge.net/. The numerical DCH calculation of the isolated Cu atom was performed using the *GRASP* (*general-purpose relativistic atomic structure program*) software package (Dyall *et al.*, 1989). *SHELX97* (Sheldrick, 2008) was used for the refinement and solving of the structures. Spin and electron densities were produced using the *XCrysDen* program package (Kokalj, 1999; code available from http://www.xcrysden.org/).

4. Results and discussion

4.1. Relativistic and picture-change effects in the Cu atom

Since the compounds studied involve the elements copper and iron, we begin by investigating the relativistic and picture-change effects on the electron density of the isolated copper atom.

Fig. 2(*a*) presents the radial distribution of the Cu atom electron density at the numerical four-component DCH, the scalar UDKH2 and the NR level of theory. As is well known [see Fig. 2(*a*)], the DCH electron density close to the nucleus is larger than the NR electron density [although not obvious from Fig. 2(*a*), the numerical DCH electron density at the nucleus tends to infinity, since the point-charge model has been used in all calculations]. The UDKH2 electron density close to the nucleus is even larger than the DCH density. Close to the nucleus, *i.e.* within 0.0001 Å, the UDKH2 density is roughly twice as large as the DCH density. This large discrepancy between the DCH and UDKH2 density is presumably caused by the PCE, since the approximation owing to the termination of the DK expansion to second-order within UDKH2 has been shown to be negligible (Mastarlez *et al.*, 2008), compared with the PCE itself. Such a large difference explains the sensitivity to the PCE of those properties which are closely related to the electron density at the nucleus.

An important point to note is that the valence region is rather unaffected by the PCE. The inset of Fig. 2(*a*) shows that the relative percentage change between the UDKH2 and the exact DCH value is less than 1% for distances larger than 0.02 Å. Another important point is that, away from the nucleus, the PCE is negligible compared with the relative magnitude of the relativistic effects. Because of this the PCE in the electron density plots to be presented later will most likely not be discernible and so the PCE corrections have not been made.

The PCE in the radial distribution of the integral density $4\pi r^2\rho(r)$ is damped by the r^2 factor at small r [see Fig. 2(*b*)]. Hence the UDKH2 $4\pi r^2\rho(r)$ radial distribution closely follows

the values obtained from the DCH density, and we expect that the atomic scattering factors should be much less sensitive to the PCE than the electron density itself.

To test this, Fig. 2(*c*) shows the change in the atomic scattering factors owing to relativistic effects and PCE *versus* $\sin\theta/\lambda$. It is obvious that the PCE in the atomic scattering factors is negligible compared with the relativistic effects. Also, for $\sin\theta/\lambda > 0.25$ Å^{-1} the relativistic effects start to increase monotonically whereas the PCE decreases comparatively much more slowly on the same scale. For example, at the value of $\sin\theta/\lambda = 2$ Å^{-1} the relative change due to the relativistic effects is 1.61%, whereas the PCE influences the atomic scattering factors by only −0.08%. Thus the PCE on the atomic scattering factor is less sensitive in numerical value than the electron density itself.

It seems reasonable that the lack of sensitivity to the PCE in the atomic scattering factors of an isolated atom should also be valid in calculations of structure factors of a molecular system containing the atom (presented later).

4.2. Agreement statistics

Table 2 summarizes the results for the agreement statistics of the studied molecular systems [Fe(salpet)Cl] and [CuL_2]. It is straightforward to see that the relativistic effects on agreement statistics are much less significant than the improvement owing to the X-ray constraint. For example, the change in the weighted *R* factor owing to relativistic effects was between 0.02 and 0.04% for both compounds. These results are consistent with the localized relativistic effects seen for the isolated Cu atom. On the other hand, the improvement in the *R* factor by the X-ray constraint was 10% and 16% for the [Fe(salpet)Cl] and [CuL_2] compounds, respectively.

The χ^2 agreement statistics are rather large for the [CuL_2] compound as compared with [Fe(salpet)Cl]. On the other hand, the *R* factors for the two compounds are comparable. The origin of the large χ^2 value for the [CuL_2] compound is due to several reflections at low angle, as shown in Fig. 3. The χ^2 column of Table 2 confirms this. When χ^2 is calculated from the 10% of the structure factors with the highest $\sin\theta/\lambda$ value, denoted $\chi^2(10\%)$, we obtain values of less than 1, *i.e.* the calculated and the experimental data agree with each other within the experimental error.

The relativistic effects in the agreement statistics are small; however, the inclusion of relativistic effects (without XC) always lead to an improvement. The XC-UDKH2 model leads to the best agreement statistics.

While the effect introduced by the X-ray constraint is much higher than the relativistic effects considering the whole data set, for $\chi^2(10\%)$ the XC and relativistic effects are of comparable magnitude.

An interesting question is whether the X-ray constraint includes relativistic effects owing to the use of experimental structure factors. To test this hypothesis, the differences in χ values are compared. For the [Fe(salpet)Cl] compound the difference in $\chi(10\%)$ owing to relativistic effects only is 0.010 (*i.e.* $0.553^{1/2} - 0.538^{1/2}$), whereas the difference in $\chi(10\%)$ owing to the X-ray constraint is 0.0185. If the X-ray constraint does not include any relativistic effects, the two effects should be additive and we would predict that the decrease in $\chi(10\%)$ for XC-UDKH2 would be 0.0286 (0.0101 + 0.0185). The actual value has decreased by 0.0260, which is different from the predicted value by 0.0026. This seems small but it is a 25% reduction of relativistic effects only; the same analysis for the [CuL_2] compound yields similar conclusions with a value of 24% non-additivity. According to this argument, relativistic effects should be recovered by the XC calculation.

Table 2
Comparison of experimental and calculated structure factors of the studied complexes at different levels of theory using the following statistic parameters: *R* factor, weighted *R* factor, χ^2 value and $\chi^2(10\%)$ value (the 10% of highest-angle reflections and cleaned for reflections which are smaller than three times the experimental error).

Model	λ	*R*(*F*)	*wR*(*F*)	χ^2	$\chi^2(10\%)$
[Fe(salpet)Cl]					
UHF	0.0	0.0862	0.0455	1.875	0.553
UDKH2	0.0	0.0861	0.0453	1.855	0.538
XC-UHF	0.6	0.0829	0.0406	1.490	0.526
XC-UDKH2	0.6	0.0829	0.0404	1.479	0.515
[CuL_2]					
UHF	0.0	0.0612	0.0554	24.87	0.998
UDKH2	0.0	0.0603	0.0550	24.54	0.974
XC-UHF	0.4	0.0569	0.0462	17.32	0.971
XC-UDKH2	0.4	0.0565	0.0461	17.23	0.953

Fig. 4 shows the effects of relativity analysed in more detail for the [Fe(salpet)Cl] compound; in these figures all reflections with $F_j < 3\sigma_j$ have been removed. Fig. 4(*a*) shows that at larger angles the percentage of relativistic effects increases; at $\sin\theta/\lambda = 0.6$ the relativistic effects in structure factors reach up to 1%. The same holds for the atomic scattering factors (Wang *et al.*, 1996), which are with the growing value of $\sin\theta/\lambda$ more related to the electron density of core electrons. Fig. 4(*b*) shows that the relativistic effects concern mostly low-intensity reflections. Interestingly, the relativistic effect is largest in the range $0.3 < \sin\theta/\lambda < 0.5$ when judged as a fraction of experimental error σ_j [see Fig. 4(*c*)]. In this range the relativistic effects are of magnitude $\sim 0.2\sigma$. Assuming no systematic

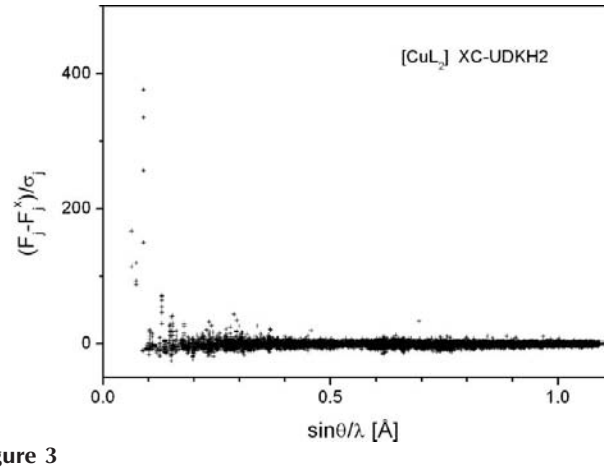

Figure 3
Difference of the measured F_j and calculated F_j^X structure factors, weighted by the experimental error σ_j for [CuL_2].

Table 3
Total SCF energies and the eigenvalue of the lowest α orbital of the studied compounds (in hartrees); the XC orbitals have not been canonicalized.

Approach		UHF	XC-UHF	UDKH2	XC-UDKH2
[Fe(salpet)Cl]	Total energy	−2766.6155	−2766.5178	−2777.3703	−2777.2755
[CuL_2]	Total energy	−2577.5000	−2576.6115	−2592.1377	−2591.2754
[Fe(salpet)Cl]	Lowest α orbital	−261.2221	−261.2776	−263.5236	−263.5753
[CuL_2]	Lowest α orbital	−328.9391	−329.6168	−332.6059	−333.1922

errors and Poisson statistics, a 25 times longer exposure time would reduce the σ values by an amount which would make these effects clearly discernible.

The ability to see relativistic effects and to test whether the XC calculation recovers this would be greatly enhanced if compounds containing heavier elements (*i.e.* 5*d*, 6*d* or lanthanides) were studied. Likewise the ability to study high-angle reflections is also desirable; this could be achieved by using synchrotron radiation at small wavelength or with γ-rays.

4.3. Effects of XC and relativity on the total energies of the studied systems

Besides the effects of relativity and X-ray constraint in electron and spin densities which are presented in the coming two sections, some considerations of the extent of XC and relativistic effects on the total self-consistent field (SCF) energy of the studied systems is presented within this section. Table 3 shows the total energies of the studied compounds at several levels of theory.

From the presented energies in Table 3 it is straightforward to see that the DKH2 approach introduces larger changes in the total energy than the X-ray constraint. In the case of [Fe(salpet)Cl] the XC-UDKH2 energy is lower than the XC-UHF energy by 10.66 hartree (atomic units, a.u.) and by 14.64 hartree for the [CuL_2] compound. Most sensitive to relativistic effects are the core electrons which become the most energetically stabilized (Pyykkö, 1988). For instance, [CuL_2] has the lowest α orbital: the eigenvalue is −332.6059 hartree at the UDKH2 level and −328.9391 hartree at the UHF level (see Table 3). Although the orbital energies presented in Table 3 were obtained using non-canonicallized orbitals (Jayatilaka, 1998), they show a very similar relativistic stabilization whether with or without the X-ray constraint. This holds for the [Fe(salpet)Cl] compound as well. The larger stabilization of the total energy of [CuL_2] by relativistic effects is explained by the larger relativistic effects in the heavier Cu atom than in the Fe and Cl atoms together. Following the work of

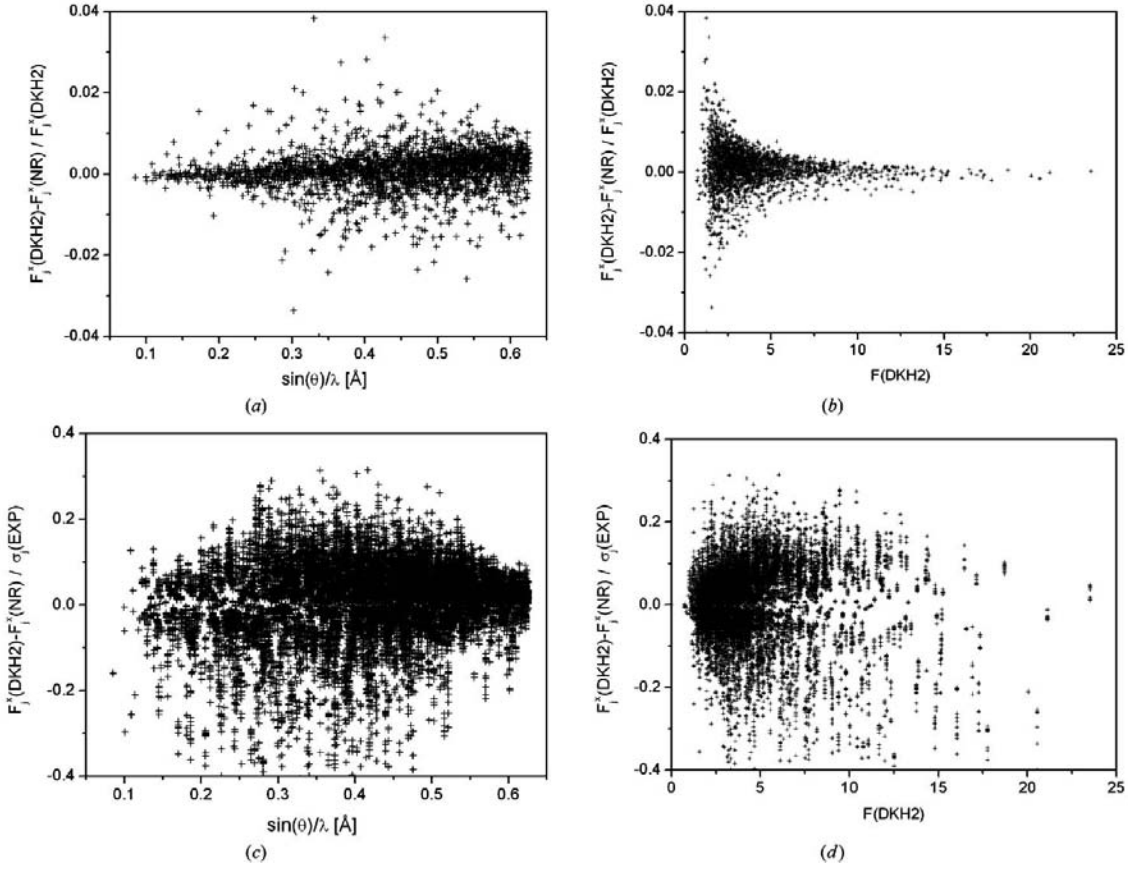

Figure 4
Relativistic effects in the calculated structure factors F_j^X of [Fe(salpet)Cl], relative to F_j^X (DKH2), plotted *versus* (*a*) $\sin\theta/\lambda$ and (*b*) F_j^X (DKH2). Relativistic effects in the calculated structure factors F_j^X of [Fe(salpet)Cl] relative to the experimental error σ_j, plotted *versus* (*c*) $\sin\theta/\lambda$ and (*d*) F_j^X (DKH2).

Desclaux (1973), the relativistic (DCH-NR) stabilization in energy for Cu is 13.75 hartree; iron together with chlorine gives 9.93 hartree. The contribution to the relativistic stabilization from the C, N and O atoms is two orders of magnitude smaller compared with iron and copper (Desclaux, 1973). The atomic data (Desclaux, 1973) were obtained from numerical DCH and NR calculations of separate open-shell atoms.

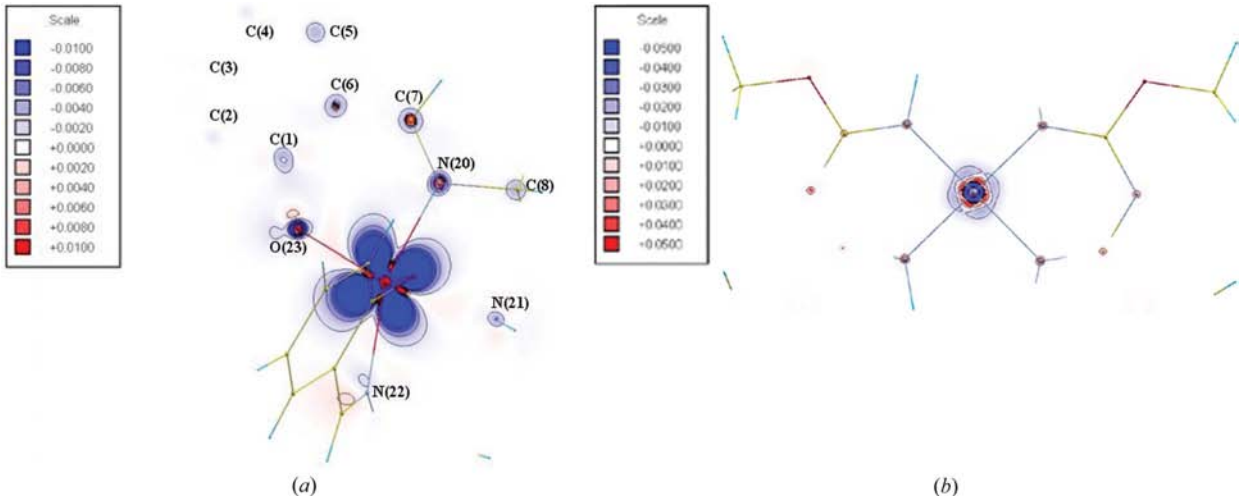

Figure 5
Difference electron density ρ(UDKH2) − ρ(UHF) showing relativistic effects in the unconstrained calculations for (*a*) [Fe(salpet)Cl] and (*b*) [CuL_2]. The difference electron densities are given in atomic units.

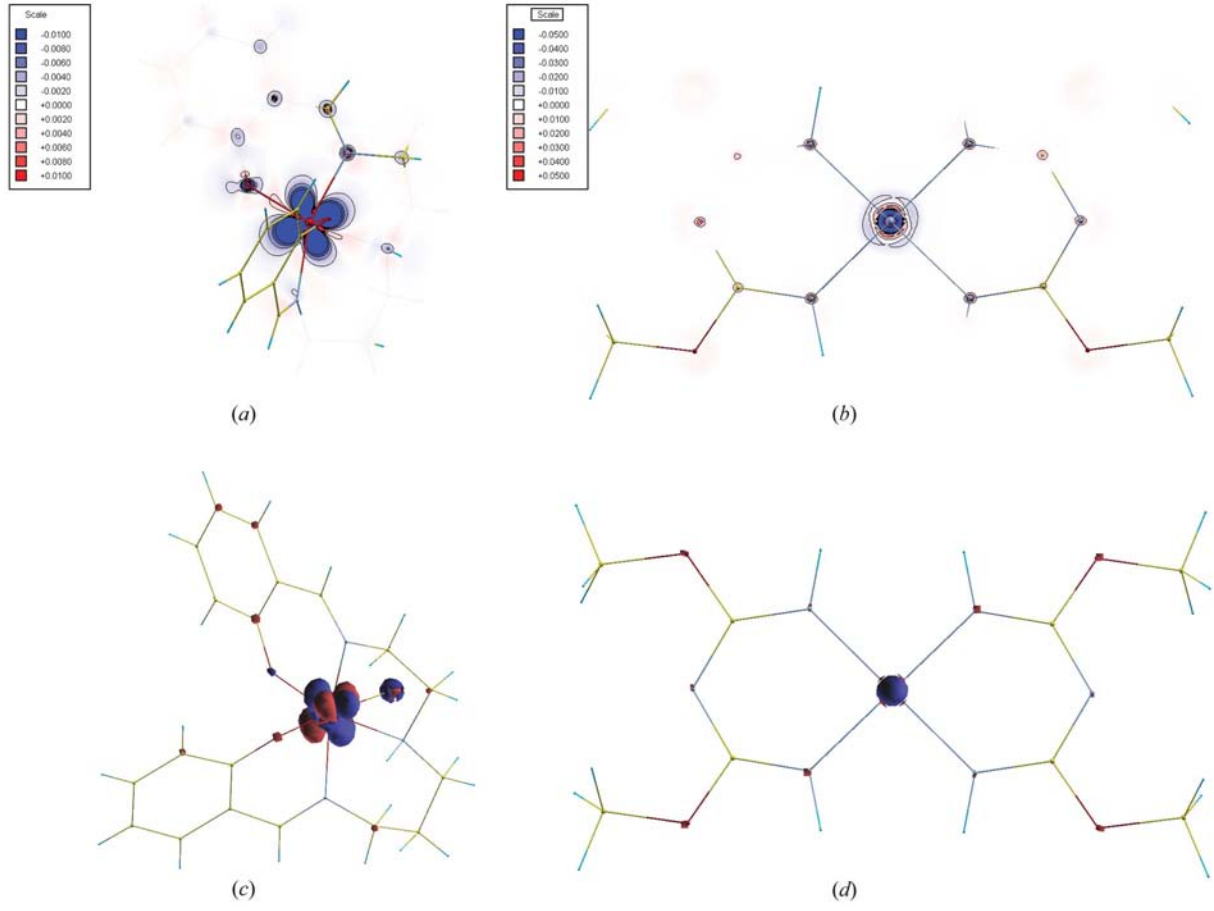

Figure 6
Difference electron density ρ(XC-UDKH2) − ρ(XC-UHF), showing relativistic effects after wavefunction fitting; (*a*) two-dimensional plot for [Fe(salpet)Cl]; (*b*) two-dimensional plot for [CuL_2]; (*c*) three-dimensional plot for [Fe(salpet)Cl], the isoline is set to 0.01 a.u.; (*d*) three-dimensional plot for [CuL_2], the isoline is set to 0.017 a.u. The two-dimensional difference electron densities are given in atomic units.

The energy shift introduced by the X-ray constraint at the UDKH2 level is only 0.095 hartree in the case of the [Fe(salpet)Cl] complex, given as the difference of the XC-UDKH2 and UDKH2 calculation. In the case of the [CuL_2] compound this change due to the constraint at the DKH2 level is an order of magnitude larger in comparison with [Fe(salpet)Cl], namely 0.862 hartree. This correlates with the high χ^2 values for the [CuL_2] compound and the large absolute change in the χ^2 value before and after XC fitting. Following the total energies in Table 3 the constraint for both compounds introduces only a slightly larger shift in energy at the NR level. The reason why the XC total energy at XC-UHF and XC-UDKH2 is higher than the usual unconstrained calculations (UDKH2 and UHF) can be explained by considering the following arguments. The variational approach of the SCF leads to the minimal energy on the energy hypersurface built of the molecular coefficients. The wavefunction fitting (XC) introduces an additional experimental constraint, but not a new variational parameter, so the energy hypersurface does not change. The molecular coefficients change within the XC approach, which have a different point on the energy hypersurface; the resulting energy becomes higher (smaller in absolute value). Moreover the XC approach is proposed to introduce the crystalline environment to a single molecule (in general a fragment); this approach is denoted as the non-interacting fragment model in the original work (Jayatilaka & Grimwood, 2001). Stabilization in the condensed phase from the interaction between the neighbouring molecules which build up the crystal is not accounted for in this model. Nevertheless, the basic motivation of the experimental constraint is a model electron density and/or wavefunction of a single molecule which resembles the crystalline environment mirroring the measured behaviour of the electron density in a crystal (like electron correlation, for instance) by the agreement with the X-ray structure factors.

4.4. Difference electron densities

Relativistic effects in the obtained unconstrained electron densities are shown in Figs. 5(*a*) and 5(*b*). As expected, the most important changes are present for the heaviest elements, Fe and Cu. Figs. 6(*a*)–6(*d*) show the relativistic effects in the constrained electron densities. Comparison of the difference electron densities in Figs. 5 and 6 shows that the relativistic effects are essentially the same regardless of the constraint; moreover, the relativistic effects on Cl can be seen in Fig. 6(*c*).

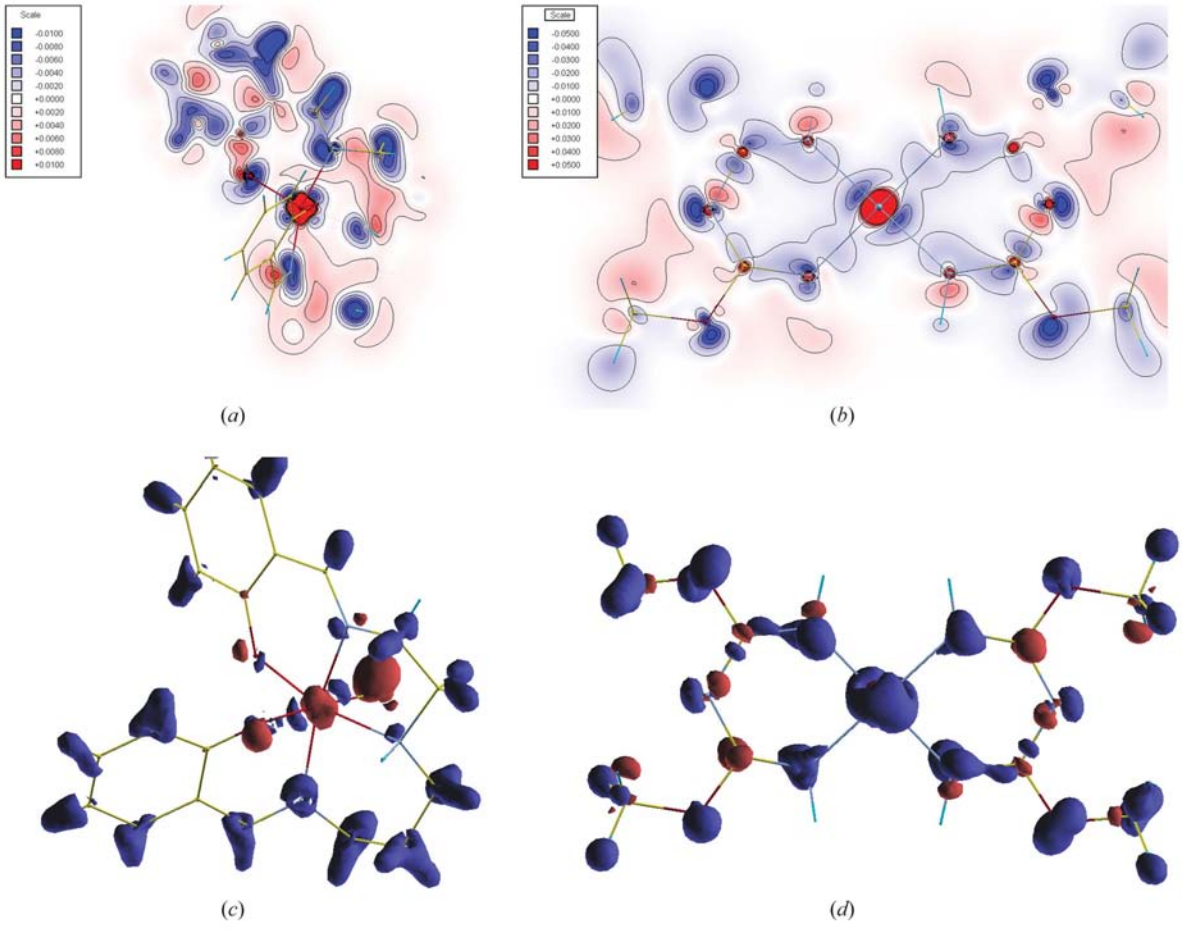

Figure 7
Difference electron densities showing the effects of wavefunction fitting ρ(XC-UDKH2) − ρ(UDKH2); (*a*) two-dimensional plot for [Fe(salpet)Cl]; (*b*) two-dimensional plot for [CuL_2]; (*c*) three-dimensional plot for [Fe(salpet)Cl], the isoline is set to 0.01 a.u.; (*d*) three-dimensional plot for [CuL_2], the isoline is set to 0.017 a.u. The two-dimensional difference electron densities are given in atomic units (Bohr^{-3}).

Previously we argued that the relativistic effects are discernible in the changes of χ statistics but clearly these changes are hardly visible to the eye in the presented electron densities.

Figs. 7(*a*)–7(*d*) show that the experimental constraint has a much bigger effect than relativity. The two-dimensional plots of difference electron density in Figs. 5(*a*)–5(*b*), 6(*a*)–6(*b*) and 7(*a*)–7(*b*) are of the same scale for each compound; the same holds for the isovalue of the three-dimensional plots in Figs. 6(*c*)–6(*d*) and 7(*c*)–7(*d*). The experimental constraint introduces significant electron redistribution on all parts of the studied molecules, see Figs. 7(*a*)–7(*d*). Since the relativistic effects (Figs. 5 and 6) are small and localized presumably on the central atoms, in the following discussion the effects of the constraint only for the UDKH2 densities are considered. The two-dimensional difference electron density plots in Figs. 7(*a*)–7(*b*) show in more detail the effects introduced by the constraint. Following the colour contours in Figs. 7(*a*)–7(*b*) are changes of electron density in the core region of atoms larger than in bonding regions. The three-dimensional difference electron density plots in Figs. 7(*c*)–7(*d*) show the regions of the largest charge density redistribution. Changes in the electron density on H atoms of the salpet ligand may be seen in Fig. 7(*c*). The electron density redistribution on the Cl atom owing to the constraint [see Fig. 7(*c*)] is visually the largest among all atoms of the [Fe(salpet)Cl] compound. The central iron and chlorine and salpet ligand atoms O(24), N(22) as well as C(8), C(10)–C(13), C(15) and C(18) undergo a change in the electron density distribution, seen in Fig. 7(*c*); the change for O(23) and N(20) seems of rather minor significance. In the case of the [CuL_2] compound most of the atoms of the ligands undergo significant charge redistribution owing to the constraint, Figs. 7(*b*)–7(*d*), which holds for H atoms of the four methyl groups as well.

4.5. Spin density

It is one of the advantages of the XC method that it can produce derived properties in a very easy way, compared with the multipole model. The spin density can be taken as a good example. The X-ray experiment and the multipole model are not able to obtain spin density from the measured structure factors. An XC spin density can be obtained as a derived property of the XC electron density which is related to the experimental structure factors. Figs. 8(*a*)–8(*d*) show the XC-UDKH2 total spin density plots of the studied compounds. The spin density at the UHF level, obtained using equation (8), contains not only regions in space of positive spin density

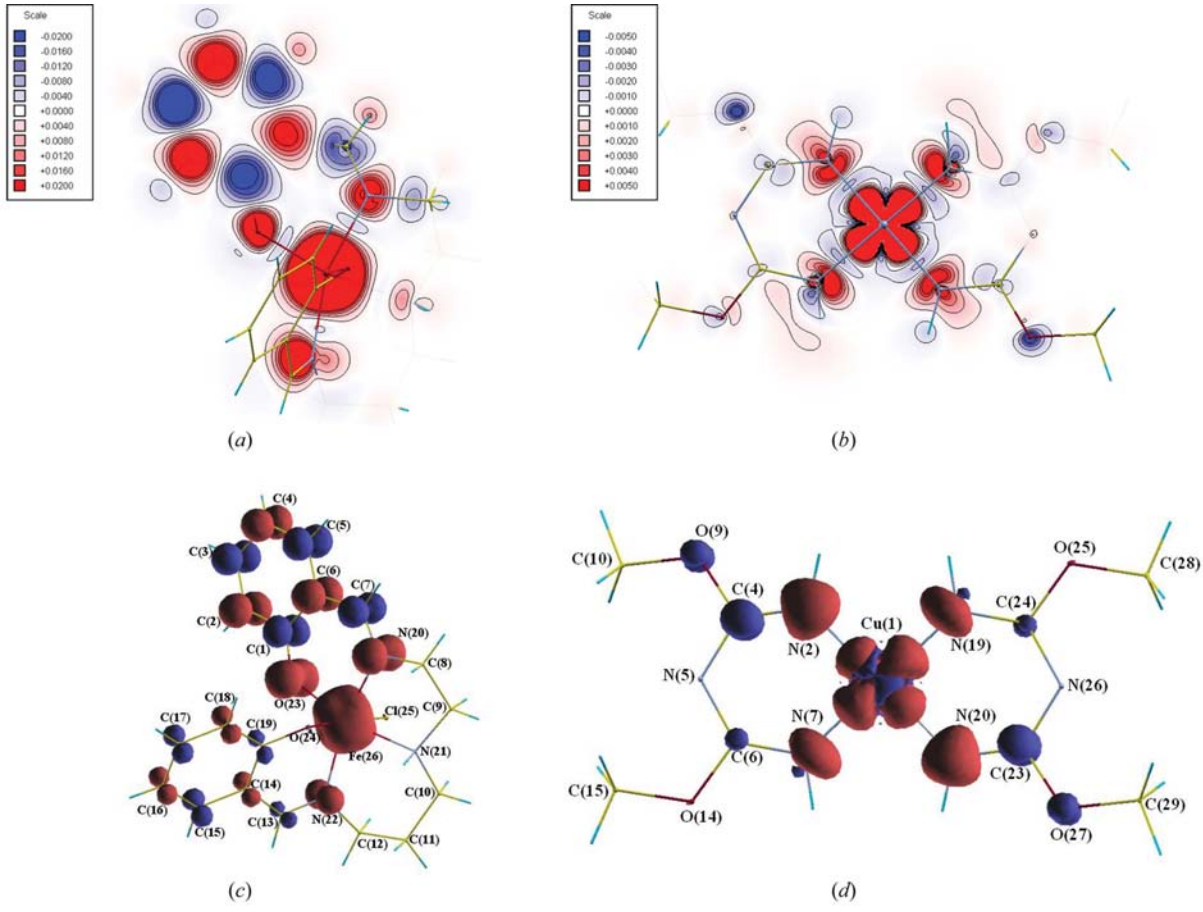

Figure 8
Spin density plots ρ_s(XC-UDKH2); (*a*) two-dimensional plot for [Fe(salpet)Cl]; (*b*) two-dimensional plot for [CuL_2]; (*c*) three-dimensional plot for [Fe(salpet)Cl], the isoline is set to 0.025 a.u.; (*d*) three-dimensional plot for [CuL_2], the isoline is set to 0.02 a.u. The two-dimensional difference spin densities are given in atomic units.

(red, where $\rho_\alpha > \rho_\beta$) but also of negative spin density (blue, where $\rho_\alpha < \rho_\beta$). The positive spin density contains the major contribution from the density of the unpaired (α) electrons, but is also enlarged by the presence of the negative spin density which has to be 'annihilated' to fulfil equation (13). The negative spin density is annihilated by means that integration of the entire spin density of equation (13) has to yield the number of unpaired electrons which have spin α.

The spin density of the [Fe(salpet)Cl] compound, shown in Figs. 8(*a*) and 8(*c*), is partially delocalized over the backbone of the salpet ligand. The actual spin of the Fe atom obtained by the Mulliken population analysis for the XC-UDKH2 calculation is 3.83 rather than the expected 5 electrons of an isolated Fe(III) atom. The three-dimensional plot of Fig. 8(*c*) shows that the major part of the delocalized spin density is found on the conjugate ring built of the C(1)–C(7), N(20) and O(23) atoms. The second conjugated ring, built of the C(13)–C(19), N(22) and O(24) atoms, contains a smaller part of the delocalized spin density. The sp^3-hybridized carbon atoms C(8)–C(12) contain only a very small amount of spin density. For instance, in Fig. 8(*a*) the spin density distribution of carbon C(8) is visible; on the other hand, the three-dimensional plot of the spin density in Fig. 8(*c*) does not show any spin density on the C(8)–C(12) carbon atoms. The Mulliken population analysis showed that the sp^3-hybridized carbon atoms C(8)–C(12) contain an order of magnitude lower amount of spin, in absolute value, compared with carbon atoms of the conjugated rings. The spin density of the second compound under study, [CuL_2], is shown in Figs. 8(*b*) and 8(*d*). Although the spin density is localized presumably on the central Cu atom, the spin density is found to be localized also on the atoms of the two ligands. The Mulliken population analysis yielded a spin of 0.846 on the Cu atom at the XC-UDKH2 level.

The relativistic effects are significant especially in the spin density around the heavy atoms; Figs. 9(*a*)–9(*d*) present the relativistic effects at the XC level. In the case of the [Fe(salpet)Cl] compound, in Fig. 9(*c*) some changes of spin density by relativistic effects are visible for the lighter atoms C(7), C(13)–C(19), N(20) and O(23), whereas the two-dimensional and three-dimensional spin densities of [CuL_2] in Figs. 9(*b*) and 9(*d*) do not present any changes at all for the lighter atoms.

Effects introduced by the constraint in the spin density for the studied compounds are presented in Figs. 10(*a*)–10(*d*).

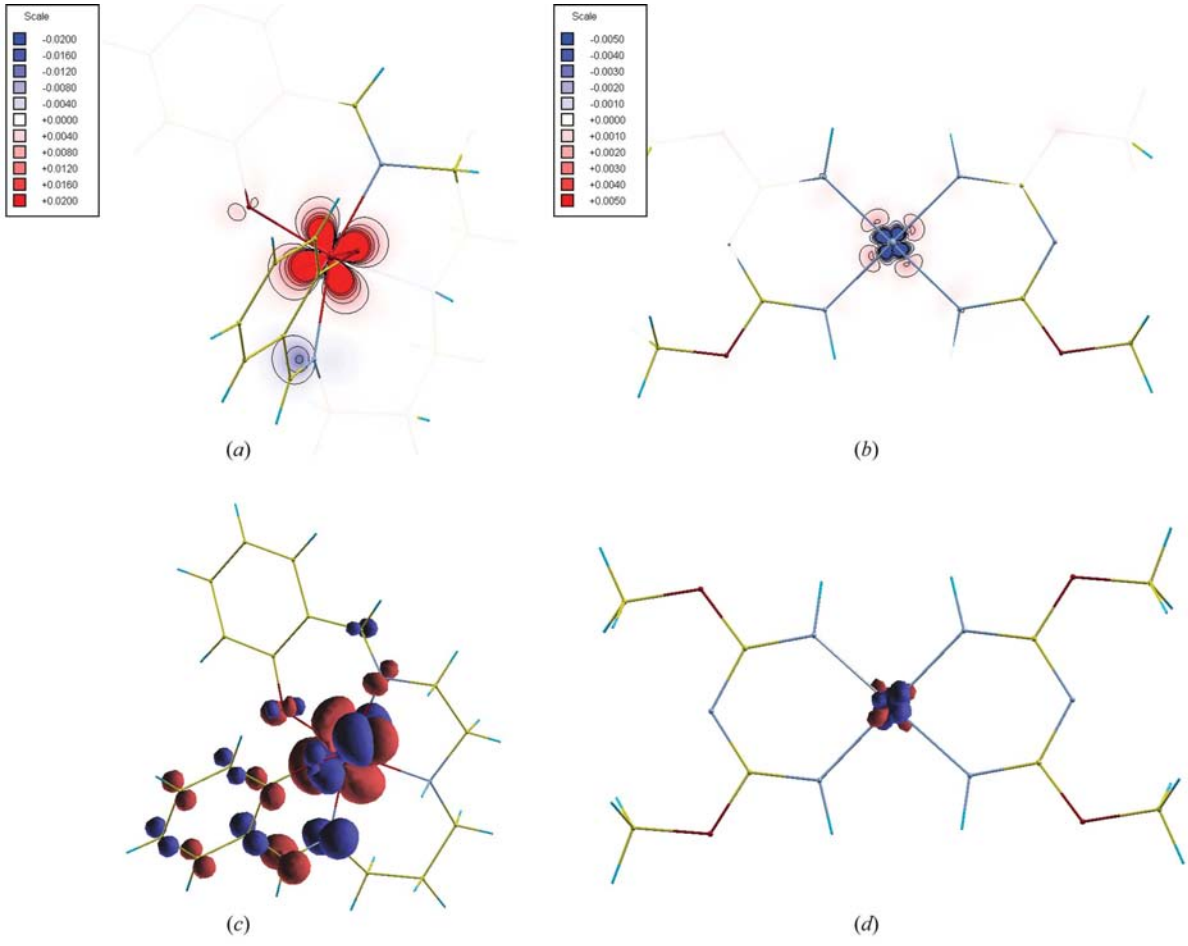

Figure 9
Difference spin density ρ_s(XC-UDKH2) − ρ_s(XC-UHF), showing relativistic effects after wavefunction fitting; (*a*) two-dimensional plot for [Fe(salpet)Cl]; (*b*) two-dimensional plot for [CuL_2]; (*c*) three-dimensional plot for [Fe(salpet)Cl], the isoline is set to 0.001 a.u.; (*d*) three-dimensional plot for [CuL_2], the isoline is set to 0.002 a.u. The two-dimensional difference spin densities are given in atomic units.

Compared with relativistic effects the constraint effects are considerably larger. In the case of [Fe(salpet)Cl] the constraint affects not only the spin density on the central iron atom but also appears to damp the spin density on the atoms C(13)–C(19), N(22) O(24) on one of the conjugated rings. This explains why the spin density on this ring is smaller in Fig. 8(*c*) and implies how sensitive spin density is to crystalline environment. It has to be noted that the difference spin densities of [Fe(salpet)Cl] in Figs. 9(*c*) and 10(c) are plotted with a 20 times smaller isoline value compared with the total spin density plot in Fig. 8(*a*). In the case of [CuL_2] a similar damping effect is introduced by the constraint [see Figs. 10(*b*) and 10(*d*)]. The spin density in Figs. 8(*b*) and 8(*d*) is less symmetric than one would expect and this can be explained by redistribution owing to the crystal environment, which is introduced by the constraint, in Figs. 10(*b*) and 10(*d*). Although the relativistic and constraint effects are of similar magnitude on the central atoms of Fe and Cu in the studied compounds, the spatial redistribution of these effects is different.

5. Conclusions

We have extended the constrained wavefunction procedure to deal with open-shell and scalar relativistic effects; both are necessary for treating heavy systems. Our first study on the [Fe(salpet)Cl] and [CuL_2] compounds has suggested that relativistic effects can be seen in the χ^2 value of the high-angle data, although the effects are small. We have found that the effect of the crystal environment (*i.e.* the X-ray constraint) is typically much larger than the relativistic effects in plots of the electron and spin density. An important aspect of this work is the first analysis of spin density at the level of X-ray constraint. The reliability of the XC-UHF spin density should be proved by a comparison with spin densities obtained from experimental and constrained polarized neutron data. The polarized neutron constrained UHF method is within the scope of the authors. Moreover, the PCE was investigated for the Cu atom and was found to be highly localized at the nucleus, and was shown to be small and damped for the atomic scattering factors.

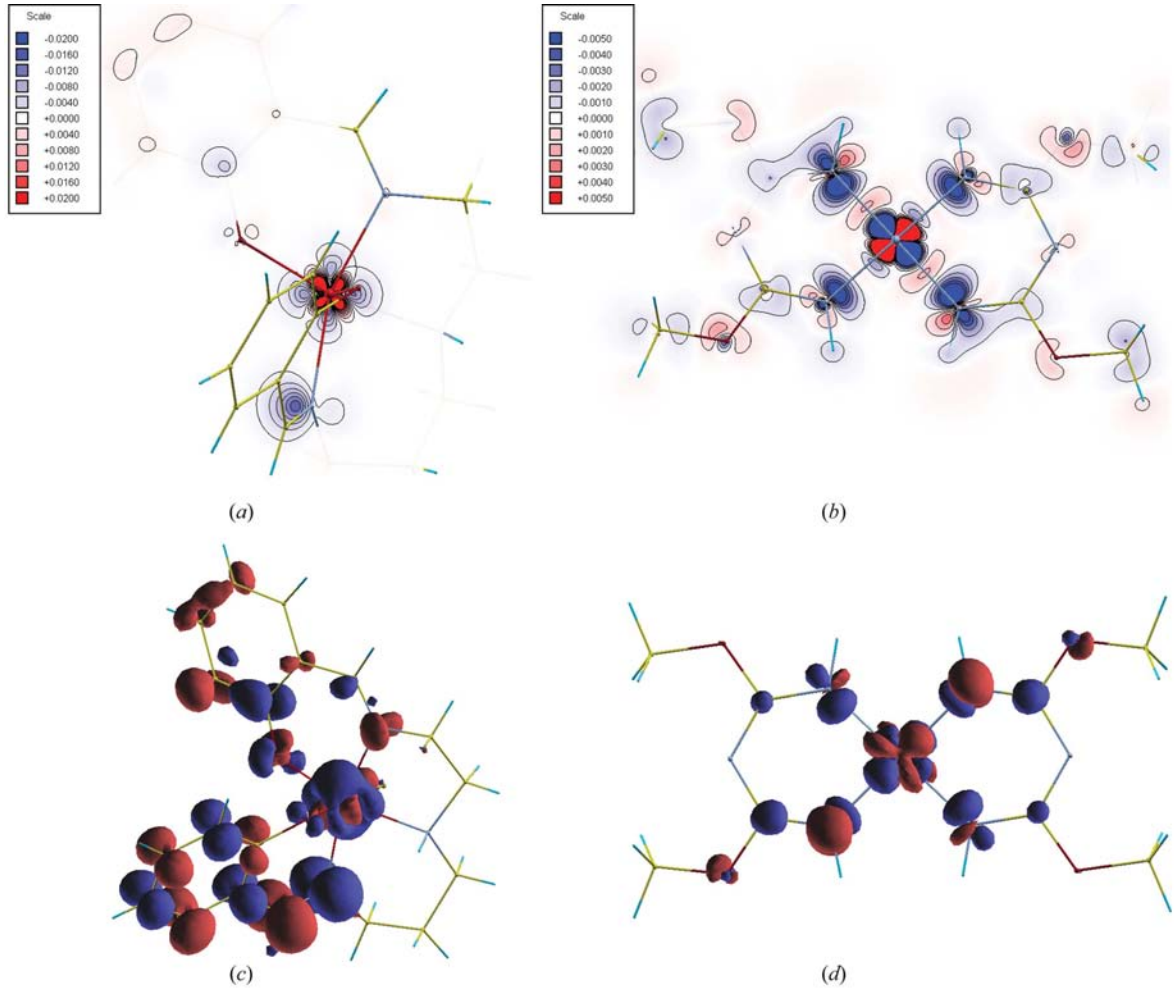

Figure 10
Difference spin densities showing the effects of wavefunction fitting ρ_s(XC-UDKH2) − ρ_s(UDKH2); (*a*) two-dimensional plot for [Fe(salpet)Cl]; (*b*) two-dimensional plot for [CuL_2]; (*c*) three-dimensional plot for [Fe(salpet)Cl], the isoline is set to 0.001 a.u.; (*d*) three-dimensional plot for [CuL_2], the isoline is set to 0.002 a.u. The two-dimensional difference electron densities are given in atomic units.

It would be interesting to see whether relativistic effects could be detected in heavy-atom compounds, where these effects are larger. A study of compounds containing Ir and Pt atoms is in the focus of the authors. It is also interesting to examine the PCE in electron and spin density as well as structure factors in more detail, especially for heavy-atom compounds. The rigorous PCE correction of electron densities and structure factors should become the topic of forthcoming papers.

In addition, the implementation of the two-component DKH2 Hamiltonian, within the general complex Hartree–Fock approach, has been completed. The basic motivation of the implementation of the two-component approach is the proper description of the real spin–orbit symmetry, which governs in the heavy elements. The XC-HF will have to be extended to cope with the two-component wavefunction to examine the importance of spin–orbit coupling in heavy-atom compounds.

This work is a part of the bilateral project: 'The extraction of microscopic information on electronic structure of molecules from experimental diffraction data, Bil/Austr/SR/STU/06'. This work was supported by Science and Technology Assistance Agency under the contract No. APVV-0093-07. The Slovak Grant Agency VEGA (contracts Nos. 1/0817/08 and 1/0127/09) is acknowledged for partial financial support. We would like to thank ARC and CNRS for funding. This work has benefited from the Center of Excellence Programme of the Slovak Academy of Sciences in Bratislava, Slovakia (COMCHEM, Contract No. II/1/2007). We are also grateful for the National Scholarship Program of the Slovak Academic Information Agency (NSP-SAIA).

References

Aebersold, M. A., Gillon, B., Plantevin, O., Pardi, L., Kahn, O., Bergerat, P., von Seggern, I., Tuczek, F., Öhrström, L, Grand, A. & Lelièvre-Berna, E. (1998). *J. Am. Chem. Soc.* **120**, 5238–5245.

Andrews, J. S., Jayatilaka, D., Bone, R. G. A., Handy, N. C. & Amos, R. D. (1991). *Chem. Phys. Lett.* **183**, 423–431.

Aronica, C., Jeanneau, E., El Moll, H., Luneau, D., Gillon, B., Goujon, A., Cousson, A., Carvajal, M. A. & Robert, V. (2007). *Chem. Eur. J.* **13**, 3666–3674.

Balabanov, N. B. & Peterson, K. A. (2005). *J. Chem. Phys.* **123**, 064107.

Balabanov, N. B. & Peterson, K. A. (2006). *J. Chem. Phys.* **125**, 074110.

Barone, G., Mastalerz, R., Reiher, M. & Lindh, R. (2008). *J. Phys. Chem. A*, **112**, 1666–1672.

Barysz, M. & Sadlej, A. J. (2001). *J. Mol. Struct. THEOCHEM*, **573**, 181–200.

Boča, R., Hvastijová, M., Kožíšek, J. & Valko, M. (1996). *Inorg. Chem.* **35**, 4794–4797.

Buenker, R. J., Chandra, P. & Hess, B. A. (1984). *Chem. Phys.* **84**, 1–9.

Cassam-Chenaï, P. & Chandler, G. S. (1993). *Int. J. Quantum Chem.* **46**, 593–607.

Desclaux, J. P. (1973). *Atom. Data Nucl. Data Tables*, **12**, 311–406.

Douglas, M. & Kroll, N. M. (1974). *Ann. Phys.* **82**, 89–155.

Dunning, T. H. Jr (1989). *J. Chem. Phys.* **90**, 1007–1023.

Dyall, K. G. & Faegri, K. (2007). *Introduction to Relativistic Quantum Chemistry.* Oxford University Press.

Dyall, K. G., Grant, I. P., Johnson, C. T., Parpia, F. A. & Plummer, E. P. (1989). *Comput. Phys. Commun.* **55**, 425–456.

Dyall, K. G. & van Lenthe, E. (1999). *J. Chem Phys.* **111**, 1366–1372.

Eickerling, G., Mastalerz, R., Herz, V., Himmel, H. J., Scherer, W. & Reiher, M. (2007). *J. Chem. Theory Comput.* **3**, 2182–2197.

Figgis, B. N., Iversen, B. B., Larson, F. K. & Reynolds, P. A. (1993). *Acta Cryst.* B**49**, 794–806.

Foldy, L. L. & Wouthuysen, S. A. (1950). *Phys. Rev. A*, **78**, 29–36.

Grimwood, D. J., Bytheway, I. & Jayatilaka, D. (2003). *J. Comput. Chem.* **24**, 470–483.

Grimwood, D. J. & Jayatilaka, D. (2001). *Acta Cryst.* A**57**, 87–100.

Hehre, W. J., Ditchfield, R. & Pople, J. A. (1972). *J. Chem. Phys.* **56**, 2257–2261.

Hess, B. A. (1985). *Phys. Rev. A*, **32**, 756–763.

Hohenberg, P. & Kohn, W. (1964). *Phys. Rev. B*, **136**, 864–871.

Ilias, M. & Saue, T. (2006). *J. Chem. Phys.* **126**, 064102.

Jayatilaka, D. (1998). *Phys. Rev. Lett.* **80**, 798–801.

Jayatilaka, D. & Grimwood, D. J. (2000). *TONTO. A Research Tool for Quantum Chemistry.* The University of Western Australia, Nedlands, Western Australia, Australia. (http://www.theochem.uwa.edu.au/tonto or http://sourceforge.net/svn/?group_id=149648.)

Jayatilaka, D. & Grimwood, D. J. (2001). *Acta Cryst.* A**57**, 76–86.

Jayatilaka, D. & Grimwood, D. (2004). *Acta Cryst.* A**60**, 111–119.

Jayatilaka, D., Munshi, P., Turner, M. J., Howard, J. A. K. & Spackman, M. A. (2009). *Phys. Chem. Chem. Phys.* doi:10.1039/b906072c.

Kellö, V. & Sadlej, A. J. (1990). *J. Chem. Phys.* **93**, 8122–8132.

Kellö, V. & Sadlej, A. J. (1995*a*). *Theor. Chim. Acta*, **84**, 353.

Kellö, V. & Sadlej, A. J. (1995*b*). *Theor. Chim. Acta*, **94**, 93–104.

Kellö, V., Sadlej, A. J. & Hess, B. A. (1996). *J. Chem. Phys.* **105**, 1995–2003.

Kokalj, A. (1999). *J. Mol. Graph. Model.* **17**, 176–179.

Lenthe, E. van, Baerends, E. J. & Snijders, J. G. (1993). *J. Chem. Phys.* **99**, 4597–4610.

Lenthe, E. van, Baerends, E. J. & Snijders, J. G. (1994). *J. Chem. Phys.* **101**, 9783–9792.

Malkin, I., Malkin, O. L. & Malkin, V. G. (2002). *Chem. Phys. Lett.* **361**, 231–236.

Malkin, I., Malkin, O. L., Malkin, V. G. & Kaupp, M. (2004). *Chem. Phys. Lett.* **396**, 268–276.

Mastarlez, R., Lindth, R. & Reiher, M. (2008). *Chem. Phys. Lett.* **465**, 157–164.

Nakajima, T. & Hirao, K. (2000). *J. Chem. Phys.* **113**, 7778–7786.

Norman, P., Schimmelpfennig, B., Ruud, K., Jensen, H. J. Å. & Ågren, H. (2002). *J. Chem. Phys.* **116**, 6914–6923.

Parr, R. G. & Yang, W. (1989). *Density-Functional Theory of Atoms and Molecules*. New York: Oxford University Press.

Peterson, K. A., Figgen, D., Dolg, M. & Stoll, H. (2007). *J. Chem. Phys.* **126**, 124101.

Pople, J. A., Gill, P. M. & Handy, N. C. (1995). *Int. J. Quantum Chem.* **56**, 303–305.

Pyykkö, P. (1988). *Chem. Rev.* **88**, 563–594.

Reiher, M. (2006). *Theor. Chem. Acc.* **116**, 241–252.

Reiher, M. (2007). *Faraday Discuss.* **135**, 97–124.

Reiher, M. & Wolf, A. (2004*a*). *J. Chem. Phys.* **121**, 2037–2047.

Reiher, M. & Wolf, A. (2004*b*). *J. Chem. Phys.* **121**, 10945–10956.

Šalitroš, I., Boča, R., Dlháň, Ľ., Gembický, M., Kožíšek, J., Linares, J., Moncol', J., Nemec, I., Perašínová, L., Renz, F., Svoboda, I. & Fuess, H. (2009). *Eur. J. Inorg. Chem.* pp. 3141–3154.

Schwerdtfeger, P. (2002). Editor. *Relativistic Electronic Structure Theory, Part 1. Fundamentals.* Amsterdam: Elsevier.

Sheldrick, G. M. (2008). *Acta Cryst.* A**64**, 112–122.

Stevens, E. D. & Coppens, P. (1976). *Acta Cryst.* A**32**, 915–917.

Szabo, A. & Ostlund, N. S. (1989). *Modern Quantum Chemistry: Introduction to Advanced Electronic Structure Theory*, 1st ed., revised. New York: McGraw-Hill.

Wang, J., Smith, V. H., Bunge, C. F. & Jáuregui, R. (1996). *Acta Cryst.* A**52**, 649–658.

Whitten, A. E., Jayatilaka, D. & Spackman, M. A. (2006). *J. Chem. Phys.* **125**, 174505.
Whitton, A. (2004). Honours thesis, University of Western Australia, Australia.
Wolf, A. & Reiher, M. (2006*a*). *J. Chem. Phys.* **124**, 064102.
Wolf, A. & Reiher, M. (2006*b*). *J. Chem. Phys.* **124**, 064103.
Wolf, A., Reiher, M. & Hess, B. A. (2002*a*). *Relativistic Electronic Structure Theory, Part 1. Fundamentals*, editor P. Schwerdtfeger, pp. 622–663. Amsterdam: Elsevier.
Wolf, A., Reiher, M. & Hess, B. A. (2002*b*). *J. Chem. Phys.* **117**, 9215–9226.
Wolf, A., Reiher, M. & Hess, B. A. (2004). *Recent Advances in Relativistic Molecular Theory*, edited by K. Hirao and Y. Ishikawa, pp. 137–190. Singapore: World Scientific.
Woon, D. E. & Dunning, T. H. Jr (1993). *J. Chem. Phys.* **98**, 1358–1371.
Wüllen, C. van & Michauk, C. (2005). *J. Chem. Phys.* **123**, 204113.